Sains Malaysiana 43(2)(2014): 273–281

Synthesis and Characterization of Cu-doped ZnO Nanorods

(Sintesis dan Pencirian Cu terdop Nanorod ZnO)

S.Y. PUNG*, C.S. ONG, K. MOHD ISHA & M.H. OTHMAN

ABSTRACT

Cu-doped ZnO nanorods were synthesized by sol-gel method using zinc nitrate tetrahydrate, methenamine and cupric acetate monohydrate as precursors. The as-synthesized ZnO nanorods have a twin-rod structure. The polar (002) surface of ZnO nanorods, which could be either negatively charge (O-terminated) or positively charged (Zn-terminated), was responsible for the formation of twin-rod structure. The results showed that the size, aspect ratio, crystallinity and c-lattice parameter of Cu doped ZnO nanorods decreased with increasing of Cu dopant concentration. In fact, the presence of Cu retarded the growth of ZnO nanorods in its preferred growth direction, i.e. (0001). The XPS analysis indicates that Cu ions were oxidized (Cu^{2+}) and substituted into the ZnO lattice at the Zn^{2+} site. The presence of Cu reduced the optical bandgap of ZnO from 3.34 eV (undoped ZnO nanorods) to 3.31 eV (20 mol% Cu doped ZnO). Besides, it induced a visible PL emission at 2.97 eV, which could be related to the transition of electrons from conduction band (E_c) to Cu acceptor energy level (E_v + 0.45 eV) radiatively.

Keywords: Copper; in-situ *doping; semiconductor; sol-gel processes; ZnO nanorods*

ABSTRAK

Cu terdop nanorod ZnO telah disintesis dengan kaedah sol-gel dengan menggunakan zink nitrat tetrahidrat, metenamin dan kuprik asetat monohidrat sebagai prapenanda. Nanorod ZnO yang disintesis ini mempunyai struktur rod berkembar. Permukaan (002) nanorod ZnO yang berkutub, sama ada caj negatif (dipangkalkan oleh O) atau caj positif (dipangkalkan oleh Zn), bertanggungjawab untuk pembentukan struktur rod berkembar ini. Keputusan menunjukkan bahawa saiz, nisbah bidang, kehabluran dan parameter kekisi-c Cu-dop nanorod ZnO ini menurun dengan meningkatnya pendopan kepekatan Cu. Sebenarnya, kehadiran Cu menghalang pertumbuhan nanorod ZnO dalam halaan pertumbuhan yang diutamakan, iaitu (0001). Analisis XPS menunjukkan bahawa ion Cu telah dioksidakan (Cu^{2+}) dan digantikan dalam kekisi ZnO di kedudukan Zn^{2+}. Kehadiran Cu juga mengurangkan jalur tenaga optikal ZnO daripada 3.34 eV (nanorod ZnO tanpa dop) ke 3.31 eV (20 mol% ZnO Cu terdop). Tambahan lagi, ia menghasilkan pancaran PL di 2.97 eV, yang boleh dikaitkan dengan peralihan elektron dari jalur konduksi (E_c) kepada paras tenaga Cu penerima (E_v + 0.45 eV) secara radiatif.

Kata kunci: Kuprum; nanorod ZnO; pendopan in-situ*; proses sol-gel; semikonduktor*

INTRODUCTION

Undoped ZnO semiconductor has a bandgap of 3.37 eV and emits UV light with wavelength ~368 nm. The single color light emission of ZnO limits its application in opto-electronic fields. This issue could be addressed by altering the bandgap energy of ZnO. Doping is one of the alternative approaches to alter the bandgap energy of ZnO either by narrowing the bandgap or by introducing energy levels in the bandgap of semiconductor materials. For instance, by doping impurities such as Mn, Cr and Co, ZnO with wavelength could be tuned to visible light region was produced (Pearton et al. 2007).

Doped ZnO nanorods could be synthesized either by *ex situ* or *in situ* approach. *Ex situ* approach was achieved by coating the dopants on the as-synthesized ZnO nanorods prior to the post annealing as demonstrated by Phan et al. (2008). *In situ* approach incorporated the dopants into ZnO lattice during the synthesis process. Various *in situ* synthesis techniques had been used to produce doped ZnO. These techniques include aerosol-assisted chemical vapor deposition (AA-CVD) (Pung et al. 2010), pulsed laser deposition (PLD) (Zhang et al. 2005) and thermal evaporation (Yao et al. 2002). The inherent limitations of these techniques are high equipment and processing costs and long synthesis temperature.

In this work, *in situ* doping of Cu into ZnO nanorods were performed using sol-gel approach. Cu, which has the similarity in the electronic shell structure with Zn, was chosen as dopant due to its high solubility in ZnO. The high ionization energy of Cu and the low formation energy of substitutional group 1B elements allowed high concentration of Cu to be doped into ZnO (Khan et al. 2002; Yan et al. 2006). Cu could possibly produce p-type ZnO by introducing acceptor energy level in ZnO with energy 0.45 eV above the valence band (Xu et al. 2004).

Materials and Methods

Cu-doped ZnO nanorods were synthesized using zinc nitrate tetrahydrate (0.02 M), methenamine (0.02 M) and cupric acetate monohydrate, (0.02 M). When the temperature of solution achieved 75ºC, silicon wafers were immersed into the solution immediately for 1 h. Then, the wafers were taken out from the solution, rinsed thoroughly with DI water and dried at 100ºC for 0.5 h. The remaining white particles in the solution were washed with DI water, dried and collected for UV-Vis analysis. The effect of Cu concentration on the morphology, crystallinity and optical property of ZnO nanorods was studied. For comparison purposes, undoped ZnO nanorods were synthesized using similar synthesis condition without cupric acetate monohydrate.

The crystalline phase of the samples was determined by X-ray diffractometer (Bruker Advanced X-ray Solution D8, Cu K_{α} radiation, l = 0.154 nm). The morphology of the samples were examined by a field-emission scanning electron microscope (Zeiss Supra 35VP) attached with an energy dispersive spectroscope. The photoluminescence property of the samples was characterized by PL Spectrophotometer (Horiba JobinYvon Spectrometer HR 550, 450 W, Xe lamp, 325 nm). The optical bandgap of the samples was characterized from their absorption peak using UV-VIS Spectrophotometer (Cary 50) at room temperature. X-ray photoelectron spectroscopy (Omicron Nanotechnology, ELS 5000, non monochromatic Mg_{Ka} radiation) was used to examine the chemical bonds of these samples.

Results and Discussion

UNDOPED ZNO NANORODS

Figure 1 shows the XRD pattern of the as-synthesized sample on silicon wafer. The XRD pattern matches well with the wurtzite ZnO (JCPDS Card No: 00-001-1136). The diffraction peaks of 31.93, 34.56, 36.41, 47.94 and 56.52° can be indexed to (100), (002), (101), (102) and (110). This result indicated that the as-synthesized sample was ZnO. Two additional diffraction peaks are observed at angle 33.12 and 54.74º. These peaks were contributed by Si substrates (JCPDS Card No: 01-082-1557).

The as-synthesized particles on Si substrate were ZnO nanorods as shown in Figure 2. Agglomeration of ZnO nanorods was clearly seen in Figure 2(a). The agglomeration could be attributed to the secondary nucleation which occurred on the surface of some of the nanorods and/or the static charges that adhered ZnO nanorods in solution onto the ZnO nanorods that grown on the Si substrate. Agglomeration of nanorods could not be avoided for growing the ZnO nanorods using solution route.

As shown in Figure 2(b), most of the ZnO nanorods composed of a twin-rod structure, i.e. the nanorod was formed by two smaller nanorods that joined at the tips. This could be attributed to the polar surface of ZnO nanorods. The crystal plane of the tip of ZnO nanorods, i.e. (002), could either comprise the negatively charge O^{2-}-terminated plane or the positively charge Zn^{2+}-terminated plane. These two opposite charged surfaces could be assembled spontaneously during the crystal growth process to counterbalance the polar fields. As a result, this led to the formation of twin-rod structures. The average length, diameter and aspect ratio of undoped ZnO nanorods were 808.6±30.0 nm, 150.9±7.1 nm and 5.7±0.3, respectively.

CU-DOPED ZNO NANORODS: EFFECT OF CU CONCENTRATION

Effect of Cu dopant concentration on the growth of ZnO nanorods was studied. In this case, 1, 5, 10, 15 and 20 mol% of $Cu(CH_3CO_2)_2.H_2O$ were added into the mixture of $Zn(NO_3)_2.4H_2O$ and $(CH_2)_6N_4$ solution, respectively. The as-synthesized samples were characterized by XRD as shown in Figure 3. The XRD pattern of all the samples could

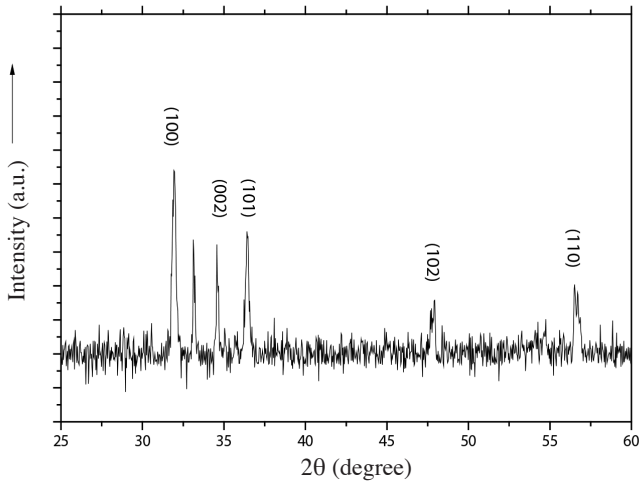

FIGURE 1. XRD pattern of undoped ZnO sample

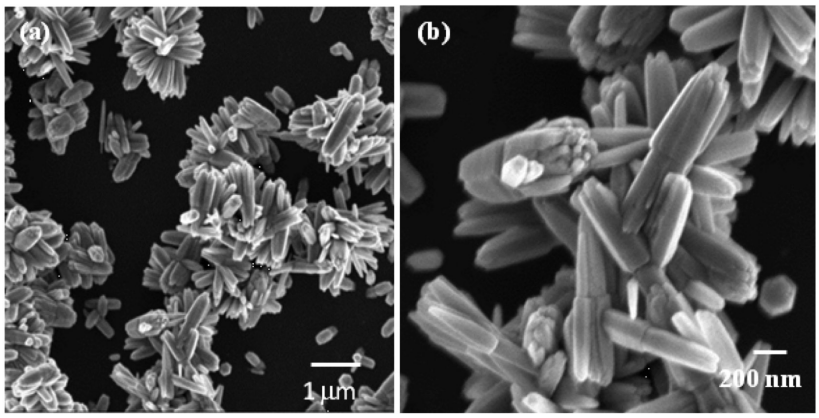

FIGURE 2. Undoped ZnO nanorods synthesized by sol-gel approach at (a) 10 kX and (b) 30 kX

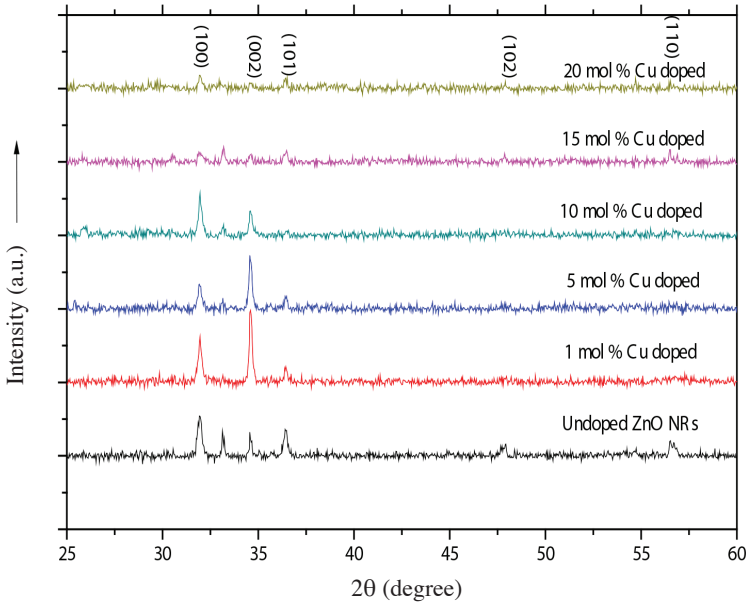

FIGURE 3. XRD pattern of Cu doped ZnO nanorods

be indexed to wurtzite ZnO (JCPDS Card No: 00-001-1136). The Cu atoms incorporated into the ZnO nanorods probably by substituting Zn in the host lattice. Besides, no second phase of impurities such as Cu or CuO was detected in all the samples. Generally, the intensity of major diffraction peaks such as (100), (002) and (101) decreased with increasing of Cu concentration. Similar observation was reported by Lee et al. (2001). They claimed that formation of the metallic copper clusters at high concentration of Cu dopant was the obstacles for the growth of ZnO nanorods. Although this might not be the case in this study, the result still clearly shown that high concentration of Cu^{2+} ions in the sol solution retarded the growth of ZnO nanorods.

Incorporation of Cu^{2+} ions into the ZnO crystal has little effect on the *a*- and *c*-lattice parameters of ZnO as the Cu^{2+} ions and Zn^{2+} ions have almost similar ionic radius which are 7.3 and 7.4 nm, respectively. However, further analysis on the lattice parameters of Cu doped ZnO nanorods, particularly the *c*-axis lattice parameter, shows a decreasing trend, i.e. from 5.1872 Å (undoped) to 5.1760 Å (20 mol% Cu) (Figure 4(a)). The *c*-lattice parameter of ZnO nanorods demonstrated a decreasing trend. No obvious trend could be observed in Figure 4(b) for the *a*-lattice parameter of ZnO nanorods doped with different concentration of Cu.

These observations could be explained from the view of dimension of ZnO nanorods (length of ZnO nanorod was longer than its diameter) and the arrangement of Zn^{2+} and O^{2-} ions in the crystal plane. ZnO crystals grow faster in (0001) (*c*-axis) attributed to its lowest surface energy as compared to other directions. More Cu dopants could be found in its *c*-axis as compared to its a-axis attributed to its longer dimension in a uniformly Cu doped ZnO nanorod. Therefore, the accumulation effect of Cu^{2+} ions

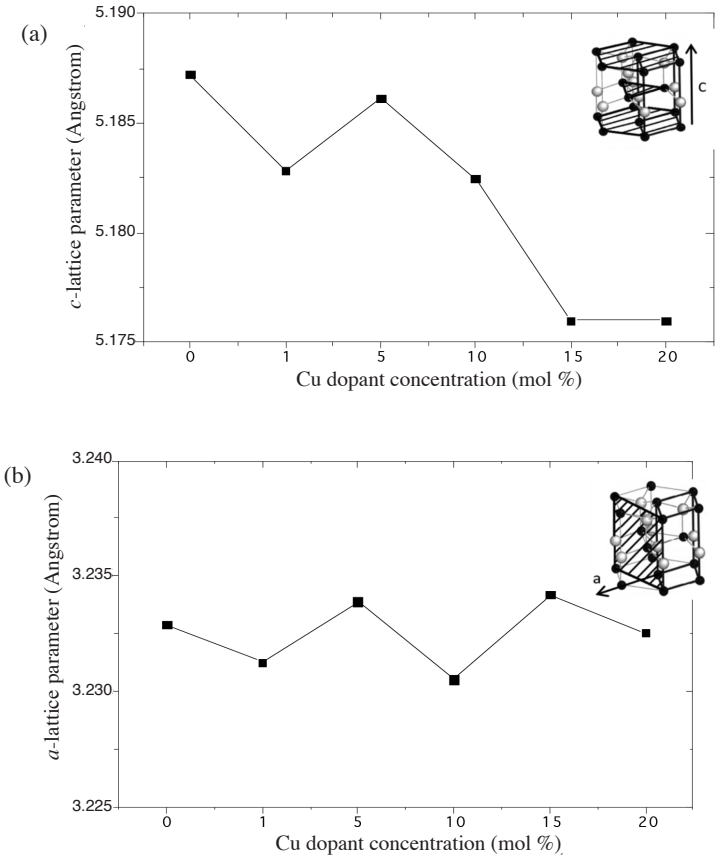

FIGURE 4. (a) *c*-lattice parameter and (b) *a*-lattice parameter of ZnO nanorods doped with different Cu dopant concentration

to reduce the *c*-lattice parameter of ZnO rod was relatively significant than in its *a*-lattice parameter. Furthermore, the (002) crystal plane (plane which perpendicular to *c*-axis) is the only crystal plane of ZnO crystal that composed of either Zn^{2+} ions or O^{2-} ions. The effect of substitution of Zn^{2+} ions by Cu^{2+} ions could be significant in changing the *c*-lattice parameters in this ZnO atomic arrangement. As shown in Figure 4(b), the effect of Cu dopant on the *a*-lattice parameters (diameter) of ZnO nanorods was not significant because of its smaller size as compared to the length of ZnO nanorods. Besides, the (100) crystal planes (crystal planes which perpendicular to the *a*-axis), composed mixture of the Zn^{2+} ions and O^{2-} ions. Reduction of *a*-lattice parameter contributed from the substitution of Zn^{2+} ions by Cu^{2+} ions could be 'average out' by the mixture of Zn^{2+} ions and O^{2-} ions in the (100) planes.

The atomic percentage of Zn, O and Cu elements present on the undoped and Cu doped ZnO nanorods were characterized using EDX as shown in Figure 5. No Cu was detected in undoped ZnO nanorods (Figure 5(a)). The atomic percentage ratio of Zn to O was approximately closed to 1:1, with slightly higher in its Zn content. The Si peak was contributed from the Si substrate. Nevertheless, Cu element was detected at 20 mol% Cu doped ZnO nanorods as shown in Figure 5(b). The EDX analysis indicates that only peaks for Zn, O, Si and Cu are present on the samples.

The Cu doped ZnO particles retained their rod-like structure with increasing concentration of Cu dopant as shown in Figure 6. Most of the nanorods were randomly deposited on substrates rather than grown on the substrates. The ZnO nanorods deposited on substrates come from solution via homogeneous nucleation, suggesting that homogenous nucleation was more dominant than heterogeneous nucleation for the growth of Cu doped ZnO nanorods in this sol-gel synthesis condition. The length of the Cu doped ZnO nanorods decreased as the Cu dopant concentration increased as shown in Figure 7(a). The length of undoped ZnO nanorods was of 808.6 ± 30.0 nm whereas the length of 20 mol% Cu doped ZnO nanorods was only 569.2±28.6 nm. The diameter of Cu doped ZnO nanorods increased as the Cu dose increased, as shown in Figure 7(b). Initially, the diameter of undoped ZnO nanorods was 150.9±7.1 nm. At 20 mol% Cu dopant concentration, the diameter of the nanorods was 311.2±11.0 nm. The aspect ratio of Cu doped ZnO nanorods kept on decreasing as the Cu dopant concentration was increasing as shown in Figure 7(c). The aspect ratio for the undoped ZnO nanorods was the highest, i.e. 5.7±0.3. As the Cu dopant concentration increased, the aspect ratio of the nanorods decreased to 1.9±0.1 nm at 20 mol% Cu dopant concentration. The above result demonstrates that Cu dopant retarded the growth of ZnO in (0001) and forced the crystals to grow

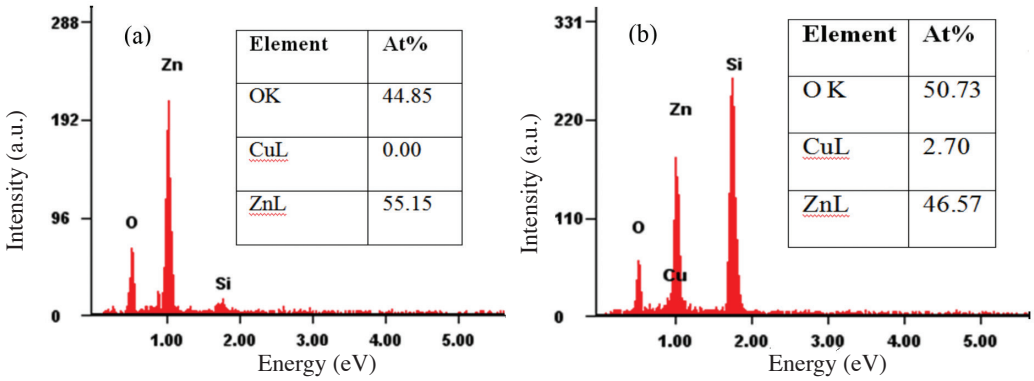

FIGURE 5. EDX analysis on (a) undoped and (b) 20 mol% Cu doped ZnO nanorods

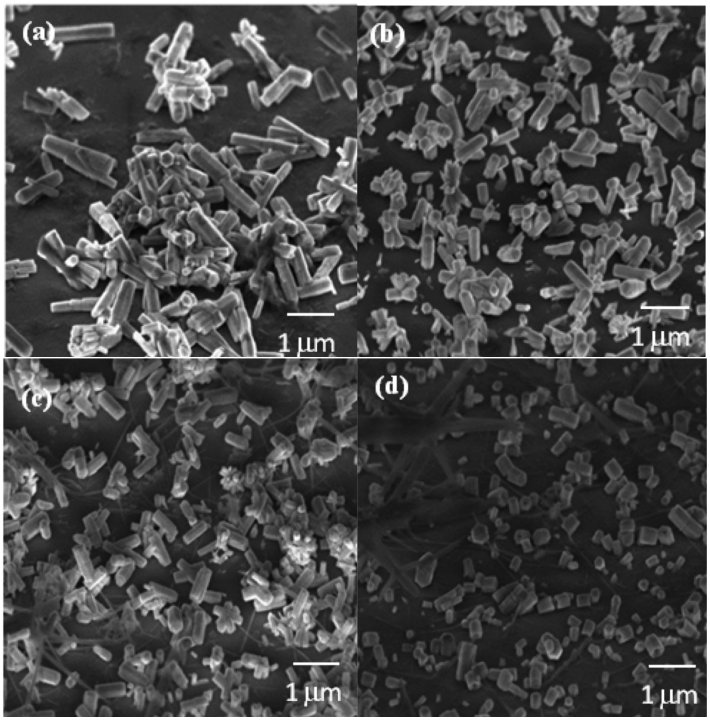

FIGURE 6. ZnO nanorods doped with different Cu dopant concentration (a) 1 mol%, (b) 5 mol%, (c) 10 mol% and (d) 15 mol%

laterally. Besides, the size (volume) of ZnO nanorods synthesized at high Cu dopant concentration (i.e. 15 mol%) was generally smaller as compared to the undoped ZnO nanorods.

Figure 8(a) shows Cu 2p core-level XPS spectra of ZnO nanorods doped with 10 mol% Cu. Two prominent peaks are observed at 933 and 953 eV which corresponding to Cu $2p^{3/2}$ and Cu $2p^{1/2}$ spin-orbit splitting, respectively. In addition, satellite peak attributed to electron shake-up of cupric oxide (Cu^{2+}) is found in the range of 940 – 945 eV (Lee et al. 2003). This indicates that Cu ions were oxidized (Cu^{2+}) in the ZnO nanorods and were substituted into the ZnO lattice at the Zn^{2+} site. The presence of Zn $2p^{3/2}$, Zn $2p^{1/2}$ and O 1s peaks at 1022.1, 1045.2 and 531.5 eV verified again that the nanorods were ZnO.

CU DOPED ZNO NANORODS: EFFECT OF ANNEALING TEMPERATURE AND ANNEALING DURATION

Post annealing was carried out to improve the crystal quality of Cu doped ZnO nanorods. The 10 mol% Cu doped samples were annealed in open air for 0.5 h at 450 and 650°C, respectively. As shown in Figure 9, the XRD pattern from each sample could be indexed into the wurtzite ZnO (JCPDS Card No: 00-001-1136). There is no sign of second phase such as metallic Cu or its oxide. Thus, post annealing did not cause formation of second phase. In addition, the diffraction intensity of major peaks such as (100), (002) and (101) of ZnO nanorods, increased with increasing post annealing temperature. This observation indicates that the crystal quality of Cu doped ZnO nanorods was improved with the increasing post annealing temperature. High post annealing temperature in open air allowed recrystallization of Cu doped

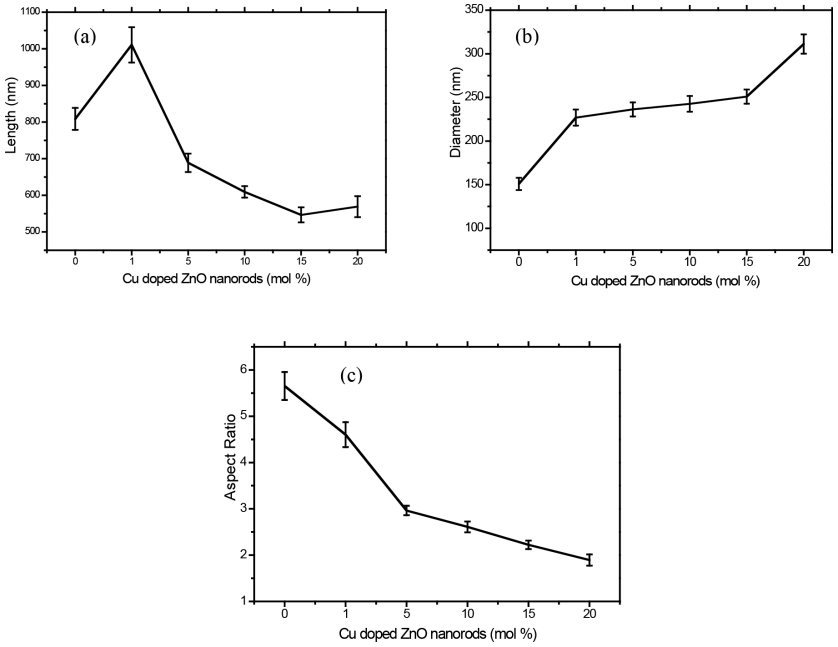

FIGURE 7. (a) Length, (b) diameter and (c) aspect ratio of Cu doped ZnO nanorods as a function of Cu dopant concentration

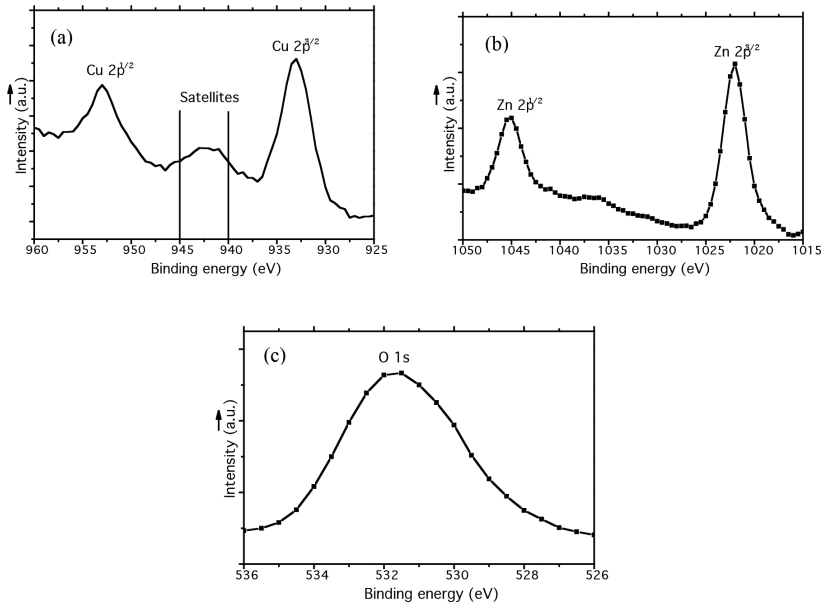

FIGURE 8. XPS spectra for (a) Cu 2p, (b) Zn 2p and (c) O 1s of Cu doped ZnO nanorods

ZnO nanorods, reducing crystal defects in ZnO such as zinc interstitials, oxygen vacancies and copper interstitials. The effect of annealing duration on the 10 mol% Cu doped ZnO nanorods was also studied. The samples were annealed at 650ºC in open air for 0.5 and 2 h, respectively. No obvious trend could be observed on the diffraction intensities of Cu doped ZnO nanorods with increasing annealing duration.

OPTICAL BANDGAP OF CU DOPED ZNO NANORODS

The optical bandgap of the Cu doped ZnO nanorods could be determined by finding the wavelength turning edge of the UV-Vis absorption peak. The optical bandgap of Cu doped ZnO nanorods as a function of Cu dopant concentration is plotted in Figure 10. The optical bandgap of ZnO nanorods decreased (red shift) with increasing of Cu dopant concentration. In this case, Cu^{2+} ions replaced Zn^{2+} ions and formed CuO in the ZnO nanorods. The CuO has a smaller bandgap (1.35 eV) as compared to ZnO (3.37 eV). Thus, when the CuO was introduced into the ZnO lattice, the intrinsic bandgap of ZnO became narrower. This result indicated that Cu was successfully doped into the ZnO nanorods as it affected the optical bandgap of

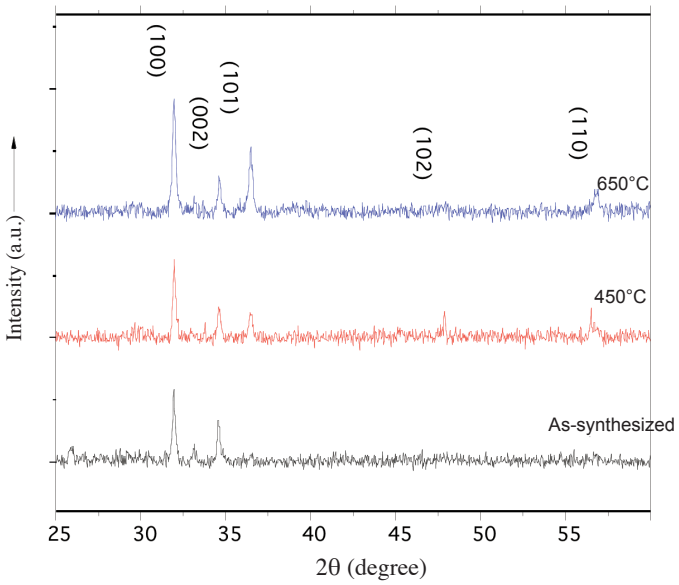

FIGURE 9. XRD pattern of 10 mol% Cu doped ZnO nanorods annealed at different temperature

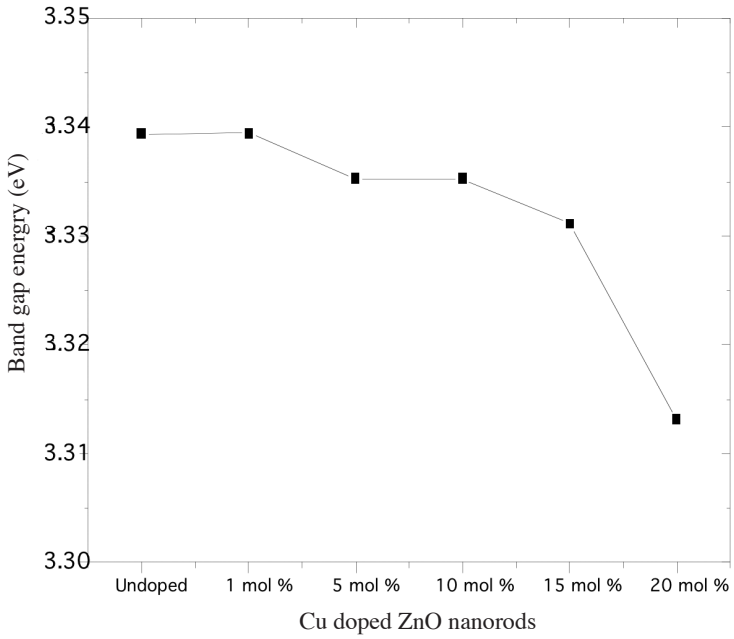

FIGURE 10. Optical bandgap energy of Cu doped ZnO nanorods

ZnO and tailoring ZnO bandgap is possible by changing the Cu dopant concentration accordingly during synthesis via sol-gel approach.

PHOTOLUMINESCENCE (PL) OF CU DOPED ZNO NANORODS

Figure 11 shows the room temperature PL spectra of undoped and Cu doped ZnO nanorods (10 mol% Cu, annealed at 650°C for 2 h). The PL spectra consist of several emissions as fitted by Gaussian distributions. The summary of the fitting is shown in Table 1. Generally, the origins of these emissions could be related to the common crystal defects in ZnO such as Zn interstitial (Zn_i), oxygen vacancy (V_o), Zn vacancy (V_{Zn}) and oxygen interstitial (O_i). The energy levels induced by these defects in the bandgap of ZnO were reported as Zn_i : E_c - 0.5 eV, V_o : E_c - 1.3 eV, V_{Zn} : E_v + 0.3 eV and O_i: E_v + 0.4 eV (E_c : conduction band, E_v : valence band) (Lee et al. 2001).

From the fittings, there are four common emissions which present in both undoped and Cu doped ZnO nanorods. The possible PL mechanisms of these four emissions could be explained as follows:

TABLE 1. Summary of the room temperature PL emissions of ZnO nanorods

Emission peak	Possible transition route	Literature reported value (eV)	Undoped ZnO nanorods (eV)	Cu doped ZnO nanorods (eV)
(a)	$E_C V_{Zn}$	3.07	3.17	3.16
(b)	$Zn_i E_V$	2.87	2.83	2.86
(c)	$Zn_i O_i$	2.47	2.39	2.43
(d)	Unknown	NA	2.24	2.23
(e)	E_C Cu acceptor level	2.92	NA	2.97

(a) The emission at 3.16-3.17 eV was related to near bandgap (NBE) emission. The radiative recombination of charge carriers occurred from the E_c to the Vz_n and subsequently relaxed non-radiatively to E_v. The photon energy at this peak was closed to the reported value, i.e. 3.07 eV;

(b) The emission at 2.83-2.86 eV was attributed to the relaxation of electrons in E_c to a lower Zn_i level non-radiatively and subsequently recombined with holes at E_v. The photon energy at this peak was closed to the reported value, i.e. 2.87 eV;

(c) The emission at 2.39-2.43 eV was contributed by the transition of electrons from Zn_i to O_i. The photon energy at this peak was closed to the reported value, i.e. 2.47 eV and

(d) The origin for the emission at 2.23-2.24 eV could not be identified. The transition of electrons from V_o to E_v produced a photon energy at 2.07 eV, which was too small as compared to the 2.23-2.24 eV.

Figure 11(b) shows the PL spectra of 10 mol% Cu doped ZnO that annealed at 650ºC for 2 h. It contained all emission peaks of undoped ZnO nanorods with additional one emission at 2.97 eV (419.16 nm, blue color). This emission could be attributed to the transition of electrons from E_c to Cu acceptor energy level radiatively and relaxed to E_v non-radiatively. The photon energy at this peak was closed to the reported value, i.e. 2.92 eV. The PL at 2.97 eV could be one of the evident to support the success of Cu doping in ZnO nanorods via sol-gel approach.

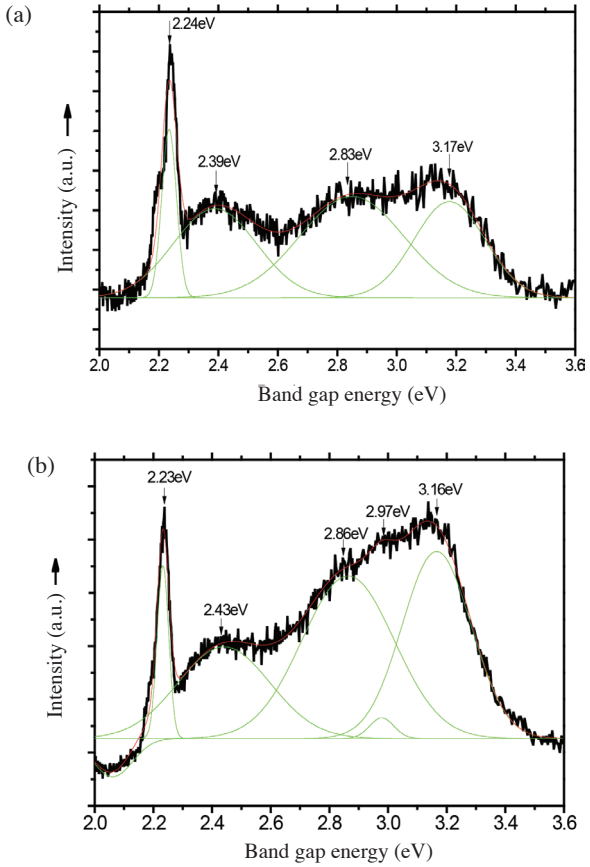

FIGURE 11. Gaussian fitting for PL spectra: (a) undoped ZnO nanorods and (b) Cu doped ZnO nanorods (10 mol% Cu, annealed at 650ºC for 2 h)

CONCLUSION

The presence of satellite peak (XPS spectra) in the region of 940 – 945 eV indicates that Cu ions were oxidized (Cu^{2+}) in the ZnO nanorods and were substituted into the ZnO lattice at the Zn^{2+} site. Substitution of a smaller Cu^{2+} ion into the ZnO lattice reduced the *c*-lattice parameter of ZnO. The increase of Cu^{2+} ions concentration in the sol solution retarded the growth of ZnO nanorods as the size and aspect ratio of ZnO nanorods became smaller. Besides, Cu doping reduced the optical bandgap of ZnO nanorods from 3.3394eV (undoped) to 3.3132eV (20 mol% Cu doped). It also induced an energy level in the bandgap at E_v + 0.45 eV.

ACKNOWLEDGEMENTS

The financial support of USM Short Term Grant (304/PBAHAN/60311011) for this project was gratefully acknowledged.

REFERENCES

Khan, S.U.M., Al-Shahry, M. & Ingler, W.B. Jr. 2002. Efficient photochemical water splitting by a chemically modified n-TiO2. *Science* 297: 2243-2245.

Lee, J.B., Le, H.J., Seo, S.H. & Park, J.S. 2001. Characterization of undoped and Cu-doped ZnO films for surface acoustic wave applications. *Thin Solid Films* 398-399: 641-646.

Lee, S.Y., Mettlach, N., Ngugen, N., Sun, Y.M. & White, J.M. 2003. Copper oxide reduction through vacuum annealing. *Appl. Surf. Sci.* 206: 102-109.

Pearton, S.J., Norton, D.P., Mil, M.P., Hebard, A.F., Zavada, J.M., Chen, W.M. & Buyanova, I.A. 2007. ZnO doped with transition metal ions. *IEEE T. Electron. Dev.* 54(5): 1040-1048.

Phan, T.L., Vincent, R., Cherns, D., Nghia, N.X. & Ursaki, V.V. 2008. Raman scattering in Me-doped ZnO nanorods (Me = Mn, Co, Cu and Ni) prepared by thermal diffusion. *Nanotechnology* 19: 475702-475706.

Pung, S.Y., Choy, K.L., Hou, X. & Dinslath, K. 2010. *In situ* doping of ZnO nanowires using aerosol-assisted chemical vapour deposition technique. *Nanotechnology* 21: 345602.

Xu, C.X., Sun, X.W., Zhang, X.H., Ke, L. & Chua, S.J. 2004. Photoluminescent properties of copper-doped zinc oxide nanowires. *Nanotechnology* 15: 856-861.

Yan, Y., Al-Jassim, M.M. & Wei, S.H. 2006. Doping of ZnO by group-IB elements. *Appl. Phys. Lett.* 89: 181912.

Yao, B.D., Chan, Y.F. & Wang, N. 2002. Formation of ZnO nanostructures by a simple way of thermal evaporation. *Appl. Phys. Lett.* 81: 757-759.

Zhang, Y.F., Russo, R.E. & Mao, S.S. 2005. Quantum efficiency of ZnO nanowire nanolasers. *Appl. Phys. Lett.* 87: 43106-43113.

S.Y. Pung* & C.S. Ong
School of Materials and Mineral Resources Engineering
Engineering Campus, Universiti Sains Malaysia
Seri Ampangan, 14300 Nibong Tebal, Pulau Pinang
Malaysia

K. Mohd Isha & M.H. Othman
Advanced Materials Research Centre, SIRIM Berhad
Lot 34, Jalan Hi-Tech 2/3, Kulim Hi-Tech Park
09000 Kulim, Kedah
Malaysia

*Corresponding author; email: sypung@eng.usm.my

Received: 7 January 2013
Accepted: 17 July 2013